This is a repository copy of *Fluidification of entanglements by a DNA bending protein*.

White Rose Research Online URL for this paper:
https://eprints.whiterose.ac.uk/194931/

Version: Accepted Version

Article:

Fosado, Yair A G, Jamieson, Howard, Weir, Simon et al. (3 more authors) (2023) Fluidification of entanglements by a DNA bending protein. Physical Review Letters. 058203. ISSN 1079-7114

https://doi.org/10.1103/PhysRevLett.130.058203

Fluidification of entanglements by a DNA bending protein

Yair A. G. Fosado,[1, *] Jamieson Howard,[2, *] Simon Weir,[1]
Agnes Noy,[2] Mark C Leake,[2, 3, †] and Davide Michieletto[1, 4, ‡]

[1]*School of Physics and Astronomy, University of Edinburgh,*
Peter Guthrie Tait Road, Edinburgh, EH9 3FD, UK
[2]*School of Physics, Engineering and Technology, University of York, York, YO10 5DD, UK*
[3]*Department of Biology, University of York, York, YO10 5DD, UK*
[4]*MRC Human Genetics Unit, Institute of Genetics and Cancer,*
University of Edinburgh, Edinburgh EH4 2XU, UK

In spite of the nanoscale and single-molecule insights into nucleoid associated proteins (NAPs), their role in modulating the mesoscale viscoelasticity of entangled DNA has been overlooked so far. By combining microrheology and molecular dynamics simulation we find that the abundant NAP "Integration Host Factor" (IHF) lowers the viscosity of entangled λDNA 20-fold at physiological concentrations and stoichiometries. Our results suggest that IHF may play a previously unappreciated role in resolving DNA entanglements and in turn may be acting as a "genomic fluidiser" for bacterial genomes.

Prokaryotic and eukaryotic genomes carry out complex biological tasks which would be impossible if randomly folded [1–5]. In bacteria, nucleoid-associated proteins (NAPs) [3] play an important role in folding the genome [3, 6–8]. Single-molecule techniques have shed light into how certain NAPs bind, bend, kink, coat or stiffen short DNA molecules in dilute conditions [7, 9–14]. However, we have little to no evidence on what is their impact on entangled and crowded DNA [6]. For instance, while DNA segregation is impaired when NAPs are removed from the cell [5, 8], the NAP-mediated mechanisms through which this segregation is achieved remain to be determined. Here, we focus on the Integration Host Factor (IHF), an abundant NAP, present at about 6,000 and 30,000 dimers per cell in E. coli during growing and stationary phase, respectively [15, 16]. IHF binds preferentially to a consensus sequence with high affinity (dissociation constant $K_d \simeq 2$nM) but also non-specifically ($K_d \simeq 2\mu$M) [17] and creates among the sharpest DNA bends in nature, up to 150° [13]. It plays a key role in horizontal gene transfer, integration and excision of phage λDNA [18] and DNA looping [19]. Recent evidence suggest that IHF may also mediate DNA bridging through non-specific, weak interactions which transiently stabilise distal DNA segments in 3D proximity [13]. Additionally, IHF appears to strengthen biofilms by interacting with extracellular DNA [20]. In light of this evidence, it remains unclear how IHF affects DNA entanglements in dense conditions, such as those of the bacterial nucleoid.

In this Letter we tackle this open question by coupling Molecular Dynamics (MD) simulations and microrheology experiments. Our MD simulations suggest that IHF can speed up the dynamics of long DNA by reducing entanglements. We validate these predictions using microrheology on solutions of entangled λDNA at volume fractions comparable to that of bacterial nucleoid ($\simeq 2\%$). Our results suggest that IHF may act as a "fluidiser" by reducing entanglements between DNA molecules and lowering the effective viscosity. By extrapolating our findings to the E. coli genome, we argue that at physiological stoichiometries IHF may reduce the effective viscosity of the nucleoid $\sim$200-fold, potentially facilitating genome reorganisation and segregation.

MD simulations of Entangled DNA with IHF – We model solutions of naked λDNA molecules using a variation of the Kremer-Grest model [21] to account for chain stiffness. We simulate M=50 coarse-grained bead-spring polymers $N = 1,000$ beads long where each bead has size $\sigma = 50$ bp, persistence length $l_p = 3\sigma = 150$ bp and volume fraction $\rho = 0.05$ (see Fig. 1a). With these choices, each polymer maps to λDNA (48,502 bp) and the expected entanglement length is $N_e \simeq 146$ beads $\simeq 7,300$ bp [22] (see SI). The beads interact via a cut-and-shift Lennard-Jones potential and are connected by FENE springs to avoid chain crossings [21]. Each chain is $N/N_e \simeq 7$ entanglement lengths long. With these choices, our systems are in the loosely entangled regime [23]. IHF dimers are modelled as permanent stiff harmonic angles constraining triplets of consecutive beads to be bent at 107° (the most frequent angle observed in AFM [13]) and we neglects unspecific bridging. The simulations are evolved with implicit solvent (Langevin dynamics) at $T = 1.0\epsilon/k_B$ and timestep $dt = 0.01\tau_{Br}$ ($\tau_{Br} = k_B T/\gamma$ is the Brownian time and γ is the friction, set to 1 in LJ units, see SI).

To model different IHF stoichiometries, we vary the number of kinks along the chains, let the systems equilibrate, and then perform a production run where we measure the properties and dynamics of the chains. The kinks are placed at random, mimicking non-specific binding. We choose to explore a range of stoichiometries that is physiologically relevant and experimentally feasible *in*
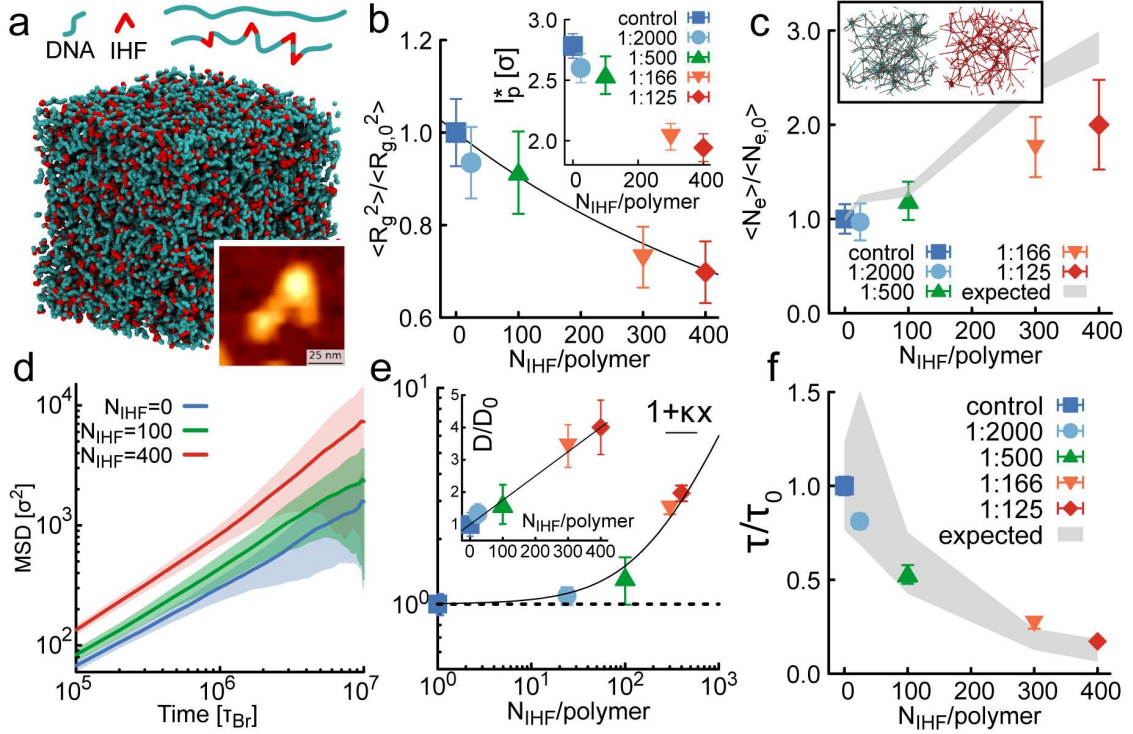
FIG. 1. **Molecular Dynamics simulations of kinked semiflexible polymers**. **a.** Snapshot of the simulation box ($M = 50$ chains $N = 1,000$ beads long with persistence length $l_p = 3\sigma$ at volume fraction $\rho = 0.05$. IHF is modelled as static and stiff harmonic angles forcing $107°$ kinks randomly placed along the chains. See also SI Movies. The inset shows an AFM image of a short DNA bound by IHF from Ref. [13]. **b.** Normalised squared radius of gyration. (inset) Effective persistence length $l_p^* = 3\langle R_g^2\rangle/N$. **c.** Entanglement length from Primitive Path Analysis. Grey shaded area represents predicted $N_e^*(l_p^*)$ with appropriate propagation of errors. (inset) Snapshots from PPA. **d.** MSD of the centre of mass of the chains. **e.** Normalised diffusion coefficient. The fitted curve is $1 + \kappa x$ with $\kappa = 0.05$ (in units of number of IHF in a polymer of 1,000 beads). **f.** Relaxation time τ defined as $MSD(\tau) \equiv \langle R_g^2\rangle$. The shaded area represents the values expected using the numerical values of N_e measured in **c** with appropriate propagation of errors.

vitro, i.e. 6,000 and 30,000 IHF dimers in growing and stationary phase [16], correspond to 1 IHF dimer every 800 and 150 bp within a 4.6 Mbp-long *E. coli* genome.

First, we observe that the more the kinks, the smaller the gyration radius of the chains $\langle R_g^2\rangle \equiv \langle 1/N \sum_i^N [\boldsymbol{r}_i - \boldsymbol{r}_{CM}]^2\rangle$ (Fig. 1b). Due to the self-avoiding interactions being screened in dense solutions [24], we estimate the size of the chain as $R_g = l_p\sqrt{N/3l_p}$, where l_p is the persistence length. In analogy with the case of freely kinked worm-like chains [25] (albeit here we set the kink to a specific angle rather than leaving a fully flexible joint as in Ref. [25]) we can renormalise the persistence length to an effective $l_p^*(N_{IHF})$ that depends on the number of kinks introduced in the chains, N_{IHF}, and compute it as $l_p^* = 3\langle R_g^2\rangle/N$. As shown in Fig. 1b(inset), the effective persistence length decreases from $l_p = 3\sigma \simeq 150$ bp to around $l_p = 1.8\sigma \simeq 90$ bp when we add 1 IHF every 2.5 beads (or 125 bp). Given that we work at fixed polymer concentration, we use l_p^* to estimate the IHF-dependent entanglement length N_e^* as [22]

$$N_e^* = l_K^* \left[\left(c_\xi \rho_K^* l_K^{*3}\right)^{-2/5} + \left(c_\xi \rho_K^* l_K^{*3}\right)^{-2}\right], \quad (1)$$

where $c_\xi = 0.06$, $l_K^* = 2l_p^*$ is the Kuhn length and $\rho_K = NM/(l_K L^3)$ is the number density of Kuhn segments. The grey shaded area in Fig. 1c shows the expected increase in entanglement length corresponding to the decrease in l_p^* predicted by Eq. (1). The actual entanglement length, measured directly via primitive path analysis (PPA) [26] (see SI), is shown as symbols. The actual increase in N_e is more moderate than the prediction yet we still observe a $\sim$ 2-fold increase, in turn halving the number of entanglements per chain, N/N_e.

To study the dynamics, we compute the mean squared displacement (MSD) of the centre of mass of the chains $g_3(t) = \langle [\boldsymbol{r}_{CM}(t + t_0) - \boldsymbol{r}_{CM}(t_0)]^2\rangle$, where the average is performed over chains and t_0. The more the kinks, the faster the dynamics (Fig. 1d) and the larger the diffusion coefficient $D = \lim_{t\to\infty} MSD/6t$. In the SI movies, one can also visually appreciate these faster dynamics.

We compute the relaxation time τ as the time at which a polymer has diffused its own size, i.e. $g_3(\tau) \equiv \langle R_g^2\rangle$ and we find a scaling compatible with reptation, i.e. $\tau/\tau_0 \sim (N/N_e)^3(N_{e,0}/N)^3 \sim (N_{e,0}/N_e)^3$ (Fig. 1f), where we used the N_e in Fig. 1c. Thus, our simulations suggest that IHF-induced kinks drive an effective increase in DNA flexibility which in turn increases the entanglement
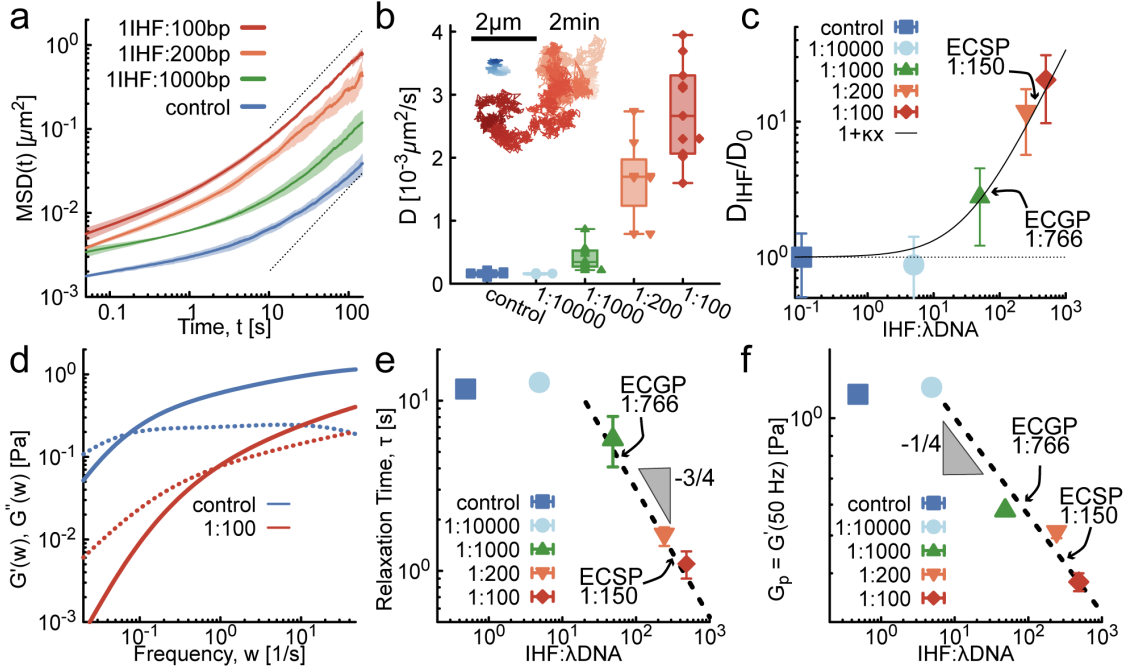
FIG. 2. **Entangled solutions of λDNA are fluidised by IHF. a.** MSDs at different stoichiometries of IHF:DNAbp. The shaded area enveloping the curves is the standard error computed over 10 movies in 3 independent experiments (> 100 tracers total). **b** Boxplot of the diffusion coefficient D from fitting $MSD = 2Dt$ at large times. (Inset) Representative particle trajectories tracked over 2 minutes. **c.** Normalised mean diffusion coefficient at increasing concentration of IHF. **d.** Complex moduli G' (solid) and G'' (dashed) for the control and for 1 IHF every 100bp. **e.** Relaxation time $\tau = w_R^{-1}$ where w_R is the crossover frequency at which $G'(w_R) \equiv G''(w_R)$. **f.** Elastic plateau obtained from the value of G' at 50 Hz. We have indicated the two biologically relevant stoichiometries in *E. coli* growing and stationary phases as "ECGP" and "ECSP".

length (as per Eq. (1)), reducing the number of entanglements per chain and speeding up the dynamics.

Microrheology of Entangled DNA with IHF – To experimentally validate our predictions, we perform microrheology [27, 28] on entangled λDNA (NEB, 48.5 kbp) at 1.5 mg/ml, corresponding to a volume fraction of $1 - 4\%$ for an effective DNA diameter $d = 5 - 10$ nm [29], valid at low salt and with $h = 0.34$ nm as the height of one basepair. This is similar to the volume fraction expected in *E. coli* nucleoid. For a 4.6 Mbp genome and $V_{nucleoid} = \pi(0.5\mu m)^2(2\mu m) \simeq 1.5\mu m^3$ we obtain $\phi \simeq 2\%$ for a $d = 5$ nm DNA diameter. Samples are made by mixing 9 μl of 1.5 mg/ml λDNA (stored in TE buffer) with 1 μl of native IHF dimers at different concentrations (stored in a 25 mM Tris pH 7.5, 550 mM KCl, 40% glycerol solution). We track the diffusion of 500 nm tracers spiked in the fluids, and extract their mean squared displacements $\langle \Delta r^2(t) \rangle$ (we have checked that larger bead sizes yield the same results, see SI). In Figs. 2a,b we show that as little as 50 IHF dimers per λDNA, or 1 IHF every 1,000 bp (comparable to 1:800 expected in growing phase), can significantly speed up the dynamics. Adding as much 1 IHF every 100 bp, speeds up the diffusion of the beads $\sim$ 20-fold. One can also visually appreciate this speed up from representative trajectories shown in Fig. 2b(inset). Pleasingly, the normalised diffusion coefficient D_{IHF}/D_0 follows the same trend as seen in simulations, i.e. $D(N_{\mathrm{IHF}}) = D_0(1 + \kappa N_{\mathrm{IHF}})$ with a linear

increase at large, yet physiological, stoichiometries (compare Figs. 2c and 1e) [30].

To further characterise the viscoelastic properties of the system, we use the generalised Stokes-Einstein relation (GSER) to compute the complex stress modulus [31] (see SI). The control sample (pure solution of λDNA at 1.5 mg/ml) displays a pronounced viscoelasticity, with a relaxation time $\tau \simeq 10$ seconds and a high-frequency elastic plateau $G_p \simeq 1$ Pa, in agreement with the values previously obtained via microrheology [28, 32] and bulk rheology [33] on similar samples (Fig. 2d). Introducing IHF at physiological stoichiometries significantly affects the rheology of the solution by both decreasing the relaxation timescale, which becomes $\tau \simeq 1$ second at 1:100 IHF:DNAbp (Fig. 2d,e), and decreasing the elastic plateau to $G_p \simeq 0.3$ Pa (Fig. 2f).

The elastic plateau G_p is related to the number of entanglements as [24, 32] $Z = L/L_e = 5MG_p/(4\rho N_A k_B T)$, with $\rho = 1.5$ mg/ml and $M = 48,502 \times 650$ g/mol the molecular weight of λDNA. We measure G_p as the value of G' at the largest frequency (50 Hz) sampled in this work. [Considering the value of G' at the crossover frequency yields the same scaling as $G'(50Hz)$ (see SI).] For our control, λDNA at 1.5 mg/ml, we find $G_p = 1.23$ Pa yielding $Z \simeq 13$ or $L_{e,0} \simeq 3,700$ bp $\simeq 1.2$ μm, in line with the one estimated for eukaryotic genomes [34].

On the other hand, by introducing IHF at 1:100 DNA bp we find that the elastic plateau yields a significantly
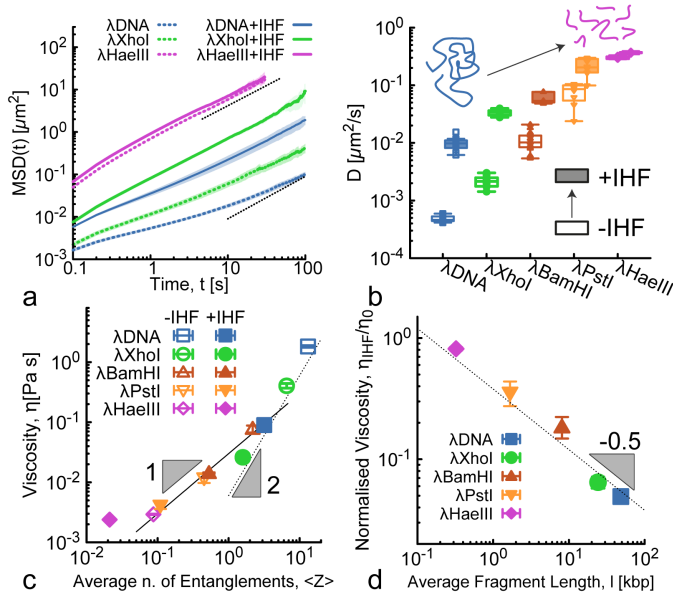
FIG. 3. **Effect of Substrate length on IHF fluidification**. **a.** MSDs of passive tracers in dense solutions of λDNA pre-digested with different restriction enzymes and before/after addition of 1 IHF every 80 bp. **b.** Diffusion coefficients of the tracer particles extracted from the large time behaviour as $MSD = 2Dt$. **c.** Viscosity η as a function of average number of entanglements per chain $\langle Z \rangle$. **d.** Normalised viscosity after/before adding IHF:80bp $\eta_{\mathrm{IHF}}/\eta_0$ plotted against average fragment length. In this figure λDNA = 0 cuts, $l = 48.5$ kbp; λXhoI = 1 cut, $l = 24.2$ kbp; λBamHI = 5 cuts, $l = 8$ kbp; λPstI = 28 cuts, $l = 1.7$ kbp; λHaeIII = 149 cuts, $l = 323$ bp. l is the average fragment length.

larger entanglement length $L_e \simeq 15,300$ bp $\simeq 5.2$ μm, corresponding to $Z \simeq 3.1$. We highlight that while the diffusion coefficient of the beads and the viscous and elastic moduli depend on the length of the polymers in solution, the entanglement length L_e does not, and it only depends on polymer concentration and stiffness [22, 26]. Thus, we can extrapolate our results to infer the level of entanglement in E. coli if no NAP or other packaging protein is present as $Z_0 \simeq L_{\mathrm{genome}}/L_{e,0} \simeq 1,200$. This implies that the expected relaxation timescale in absence of NAPs should be $\sim \tau_0 Z_0^3 \simeq 55$ years, considering a microscopic disentanglement time of order $\tau_0 = 1$ second (a typical relaxation time for solutions of marginally entangled DNA solutions with $Z \simeq 1$ [28]). It is thus clear that the bacterial nucleoid would not be able to undergo segregation unaided by NAPs and other organising proteins. Note that in Fig. 2c,e,f we have indicated the two biologically relevant stoichiometries in E. coli growing and stationary phases as "ECGP" and "ECSP".

In order to use our results to obtain insights into the impact of IHF on the viscoelasticity of the nucleoid *in vivo* we address the role of substrate length on the action of IHF. We expect that short, unentangled DNA should be insensitive to the addition of IHF, while longer and deeply entangled DNA should be more affected. To test this hypothesis we perform microrheology on dense solu-

tions (1 mg/ml) of DNA fragments with different lengths but identical overall sequence composition. The samples are obtained by digestion of λDNA via XhoI, BamHI, PstI and HaeIII, restriction enzymes that cut λDNA into 2, 6, 29 and 150 fragments, respectively. As expected, we observe that adding 1:80bp IHF to HaeIII-cut λDNA (referred to as λHaeIII) does not affect the MSD of the tracer beads (Fig. 3a). On the contrary, we observe a $\sim$20-fold speed up when IHF is introduced in full length λDNA (Fig. 3a,b) [35]. Using Stokes-Einstein, we can compute the viscosity of the samples as $\eta = k_{\mathrm{B}}T/(3\pi a D)$ and, by rescaling the average fragment length l by the entanglement length with and without IHF ($L_e = 15,300$ and $L_{e,0} = 3,700$, respectively), the values of viscosity collapse onto a master curve scaling with the average number of entanglements, $\langle Z \rangle$, as $\eta \sim \langle Z \rangle^\delta$ (Fig. 3c). The exponent $\delta = 1$ observed at small $\langle Z \rangle$ is expected for Rouse unentangled polymer solutions [24]. For $\langle Z \rangle \gtrsim 1$, our data displays a steeper scaling with $\delta = 2$. This exponent may be due to the facts that (i) we are in a crossover region to fully reptative systems ($\delta = 3$) and (ii) our systems are polydisperse [36], as they are generated by cutting λDNA with restriction enzymes [37].

Intriguingly, by plotting the ratio of the viscosity measured after and before IHF, $\eta_{\mathrm{IHF}}/\eta_0$, we observe that the speed up scales with the average length of the DNA fragments as $\eta_{\mathrm{IHF}}/\eta_0 \sim l^{-0.5}$ (Fig. 3d). To understand this we have performed MD simulations of entangled polymers of different length (see SI). We found that in the regime investigated in this work the entanglement length N_e has a dependence on the polymer length N. More specifically, by adding IHF the entanglement length increases, and the system thus needs longer chains to enter the fully entangled regime. This yields an effective scaling $N_{e,\mathrm{IHF}}/N_{e,0} \sim N^{1/4}$ (see SI). Since the viscosity can be estimated as $\eta = G_e \tau = G_e \tau_e (N/N_e)^3 \sim N_e^{-2}$, this implies that the ratio, $\eta_{\mathrm{IHF}}/\eta_0 \sim (N_{e,0}/N_{e,\mathrm{IHF}})^2 \sim N^{-0.5}$ in line with Fig. 3d.

By extrapolating this result to 4.6 Mbp long genomic DNA with about 1 IHF every 100 bp, we expect a reduction in viscosity $\eta_{\mathrm{IHF}}/\eta_0 \leq 0.01$, suggesting an effective fludification of E. coli nucleoid viscosity of about 2 orders of magnitude with respect to the case without IHF. The contribution of other NAPs, transcription factors and genome topology (e.g., supercoiling [38]) will likely affect this estimation and we hope to shed light into these other factors in future works.

Conclusions – In spite of the wealth of single-molecule evidence on how NAPs mechanically interact with short, dilute DNA, the problem of how they regulate entanglements in dense and entangled DNA solutions is poorly understood. We shed light into this problem by performing MD simulations and microrheology on dense λDNA solutions in presence of an abundant NAP called Integration Host Factor (IHF). The key discovery of this work is that IHF acts as a "fluidiser" as it reduces the

effective viscosity of entangled λDNA by 20-fold at physiological DNA concentrations and IHF:DNA stoichiometries (Figs. 1-2). Notably, we measure a quantitatively similar effect by measuring the zero-shear viscosity of DNA solutions via bulk rheology (see SI, Fig. S7). This fluidification is DNA-length-dependent and we estimate (Fig. 3) that it may shorten the relaxation time of the 4.6 Mbp-long *E. coli* genome by more than 100-fold. In the future we aim to study systems made of longer, supercoiled DNA and other NAPs such as HNS. We hope that our *in vitro* predictions will be tested *in vivo* by tracking chromosomal loci in live cells depleted of certain NAPs [39].

---

* joint first author
† co-corresponding author, mark.leake@york.ac.uk
‡ corresponding author, davide.michieletto@ed.ac.uk

[1] I. Jerkovic and G. Cavalli, Nature Reviews Molecular Cell Biology **22**, 511 (2021).

[2] R. A. Beagrie, A. Scialdone, M. Schueler, D. C. Kraemer, M. Chotalia, S. Q. Xie, M. Barbieri, I. De Santiago, L. M. Lavitas, M. R. Branco, J. Fraser, J. Dostie, L. Game, N. Dillon, P. A. Edwards, M. Nicodemi, and A. Pombo, Nature **543**, 519 (2017).

[3] S. C. Verma, Z. Qian, and S. L. Adhya, PLoS Genetics, Vol. 15 (2019) pp. 1–35.

[4] A. Japaridze, C. Gogou, J. W. Kerssemakers, H. M. Nguyen, and C. Dekker, Nature Communications **11**, 1 (2020).

[5] C. Gogou, A. Japaridze, and C. Dekker, Frontiers in Microbiology **12**, 1 (2021).

[6] A. Badrinarayanan, T. B. Le, and M. T. Laub, Annual Review of Cell and Developmental Biology **31**, 171 (2015).

[7] R. T. Dame, F. Z. M. Rashid, and D. C. Grainger, Nature Reviews Genetics **21**, 227 (2020).

[8] F. Wu, A. Japaridze, X. Zheng, J. Wiktor, J. W. Kerssemakers, and C. Dekker, Nature Communications **10**, 1 (2019).

[9] B. M. Ali, R. Amit, I. Braslavsky, A. B. Oppenheim, O. Gileadi, and J. Stavans, Proceedings of the National Academy of Sciences USA **98**, 10658 (2001).

[10] R. T. Dame, M. C. Noom, and G. J. L. Wuite, Nature **444**, 387 (2006).

[11] Y. Liu, H. Chen, L. J. Kenney, and J. Yan, Genes and Development **24**, 339 (2010).

[12] Y. Liang, R. A. Van Der Valk, R. T. Dame, W. H. Roos, and G. J. Wuite, Scientific Reports **7**, 1 (2017).

[13] S. B. Yoshua, G. D. Watson, J. A. L. Howard, V. Velasco-Berrelleza, M. C. Leake, and A. Noy, Nucleic Acids Research **49**, 8684 (2021).

[14] A. Japaridze, W. Yang, C. Dekker, W. Nasser, and G. Muskhelishvili, iScience **24**, 102408 (2021).

[15] S. C. Verma, Z. Qian, and S. L. Adhya, PLoS Genetics, Vol. 15 (2019) pp. 1–35.

[16] T. A. Azam, A. Iwata, A. Nishimura, S. Ueda, and A. Ishihama, Journal of Bacteriology **181**, 6361 (1999).

[17] S. Wang, R. Cosstick, J. F. Gardner, and R. I. Gumport, Biochemistry **34**, 13082 (1995).

[18] G. Laxmikanthan, C. Xu, A. F. Brilot, D. Warren, L. Steele, N. Seah, W. Tong, N. Grigorieff, A. Landy, and G. D. Van Duyne, eLife **5**, 1 (2016).

[19] Y. X. Huo, Y. T. Zhang, Y. Xiao, X. Zhang, M. Buck, A. Kolb, and Y. P. Wang, Nucleic Acids Research **37**, 3878 (2009).

[20] A. Devaraj, J. R. Buzzo, L. Mashburn-Warren, E. S. Gloag, L. A. Novotny, P. Stoodley, L. O. Bakaletz, and S. D. Goodman, Proceedings of the National Academy of Sciences USA **116**, 25068 (2019).

[21] K. Kremer and G. S. Grest, The Journal of Chemical Physics **92**, 5057 (1990).

[22] N. Uchida, G. S. Grest, and R. Everaers, The Journal of Chemical Physics **128**, 044902 (2008).

[23] D. C. Morse, Phys. Rev. E **58**, R1237 (1998).

[24] M. Doi and S. Edwards, The theory of polymer dynamics (Oxford University Press, 1988).

[25] P. A. Wiggins, R. Phillips, and P. C. Nelson, Phys. Rev. E **71**, 021909 (2005).

[26] R. Everaers, Science **303**, 823 (2004).

[27] T. G. Mason and D. A. Weitz, Physical Review Letters **74**, 1250 (1995).

[28] X. Zhu, B. Kundukad, and J. R. Van Der Maarel, J. Chem. Phys. **129**, 1 (2008).

[29] V. V. Rybenkov, N. R. Cozzarelli, and A. V. Vologodskii, Proc. Natl. Acad. Sci. USA **90**, 5307 (1993).

[30] We ran controls with different bead sizes, chamber cleaning protocols and post-processing algorithms. We also checked that the adsoprtion of DNA to the glass is not affecting the bulk DNA concentration (see SI for more information).

[31] T. G. Mason, Rheologica Acta **39**, 371 (2000).

[32] R. E. Teixeira, A. K. Dambal, D. H. Richter, E. S. G. Shaqfeh, and S. Chu, Macromolecules **40**, 3514 (2007).

[33] S. Banik, D. Kong, M. J. San Francisco, and G. B. McKenna, Macromolecules **54**, 8632 (2021).

[34] A. Rosa and R. Everaers, PLoS computational biology **4**, 1 (2008).

[35] Note that we consider a lagtime window of at least 20 seconds in which the exponent of the MSD is compatible with 1 (e.g. 80-100 sec). We then constrain the fit to a linear function $f(t) = 2Dt$.

[36] V. A. H. Boudara, J. D. Peterson, L. G. Leal, and D. J. Read, Journal of Rheology **63**, 71 (2019).

[37] We note that accounting for the length-dependence of L_e (becoming shorter at smaller L), the scaling may become steeper and closer to the one expected in reptation.

[38] J. Smrek, J. Garamella, R. Robertson-Anderson, and D. Michieletto, Science Advances **7**, eabf9260 (2021).

[39] A. Javer, Z. Long, E. Nugent, M. Grisi, K. Siriwatwetchakul, K. D. Dorfman, P. Cicuta, and M. Cosentino Lagomarsino, Nat. Commun. **4**, 3003 (2013).